Optics Communications 297 (2013) 102–108

Contents lists available at SciVerse ScienceDirect

Optics Communications

journal homepage: www.elsevier.com/locate/optcom

Modal properties of triangular metal groove/wedge based hybrid plasmonic structures for laser actions at deep-subwavelength scale

Yusheng Bian [a], Zheng Zheng [a,*], Xin Zhao [a], Lei Liu [a], Yalin Su [a], Jinsong Zhu [b], Tao Zhou [c]

[a] School of Electronic and Information Engineering, Beihang University, 37 Xueyuan Rd, Beijing 100191, China
[b] National Center for Nanoscience and Technology, No.11 Beiyitiao, Zhongguancun, Beijing 100190, China
[c] Department of Physics, New Jersey Institute of Technology, Newark, NJ 07102, USA

ARTICLE INFO

Article history:
Received 2 October 2012
Received in revised form
7 January 2013
Accepted 29 January 2013
Available online 26 February 2013

Keywords:
Surface plasmons
Photonic integrated circuits
Microcavity devices

ABSTRACT

Triangular metal groove/wedge based hybrid plasmonic structures are leveraged for nanolaser applications. It is shown through numerical simulations that by controlling the tip angle of the triangular metallic substrate, tunable lasing properties can be readily achieved. On the one hand, metal substrates with grooves could benefit enhanced optical confinement and meanwhile results in a reduced lasing threshold with carefully engineered tip angles. While on the other hand, metal wedge based structures could be used to further scale down the size of the stimulated optical mode, potentially enabling the realization of ultra-deep-subwavelength laser action. These novel structures could perform as efficient subwavelength light sources with flexible lasing properties, thereby facilitating diverse applications in future advanced active photonic systems.

1. Introduction

The miniaturization of optical waveguides and devices has long been a focus issue of advanced photonic systems [1]. Plasmonics, potentially being able to break the diffraction limit, has been utilized as a novel guiding mechanism for light transmission and routing at the subwavelength scale [2]. Various types of plasmonic waveguides and devices have been proposed and demonstrated for a wide range of applications from optical interconnects to sensing [3]. Recently, plasmonics have also been leveraged to fulfill the task of further downscaling of microscopic lasers, leading to the emergence of various novel nanolaser structures [4–6].

As demonstrated in the previous studies, the properties of the two dimensional plasmon lasers based on propagating surface plasmons [5] are determined strongly by the hybrid plasmonic waveguiding structures involved, which are associated with the interactions between the traditionally flat metal/dielectric surface with the cylindrical or square gain nanostructures [7–11]. Recently, a number of modified hybrid plasmonic waveguides and components have also been studied both theoretically and experimentally [12–57]. Among them, configurations with structured metallic substrates rather than the commonly employed flat metal surfaces in conventional hybrid waveguides exhibit an improved optical performance in a certain aspect. Although it might present some challenges for fabrication in a technological point of view, it is still worthwhile to see some of these unique optical properties brought by these novel substrates. For example, a vertically sandwiched semiconductor–insulator–metal waveguide on top of metal surface has resulted in a greatly reduced radiation loss for sharp bends than the hybrid structure without the additional introduced metal strip, which also brings nice optical performance when employed in passive integrated optical components [25]. On the other hand, dielectric nanowires placed above a metal wedge could lead to an enhanced mode confinement in the gap region with simultaneously mitigated propagation loss compared to the flat metal substrate based hybrid waveguides [43]. While our recent findings show that improved optical confinement could also be achieved by embedding a high-index nanowire into a thin-dielectric-coated metal *V* groove [58]. Therefore, dramatically modified modal behaviors are enabled by using these aforementioned modified hybrid structures based on structured metallic substrates, which might as well bring new capabilities when leveraged as lasing sources.

Here in this paper, we carry out a detailed investigation to reveal the possibility of using modified hybrid structures to improve the lasing properties. In the simulations, we propose to adopt a metal surface having a triangular cross-section with an angled tip as the substrate. These triangular metallic wedge/groove structures had been intensively studied as they can by themselves support highly efficient wedge plasmon polariton (WPP) [59–64] or channel plasmon polariton (CPP) modes [65–68] with appropriate geometries. These modes feature both tight light confinement and low

* Correspondence to: School of Electronic and Information Engineering, Beihang University, 37 Xueyuan Road, Haidian District, Beijing 100191, China.
Tel./fax: +86 10 8231 7220.
E-mail address: zhengzheng@buaa.edu.cn (Z. Zheng).

0030-4018/$ - see front matter © 2013 Elsevier B.V. All rights reserved.
http://dx.doi.org/10.1016/j.optcom.2013.01.075

propagation loss, and the structures could be fabricated using standard lithography methods such as Focused Ion Beam (FIB) [59] and UV lithography [61]. In our currently studied structures, the SPP modes along the metallic wall couple to the dielectric mode to form novel hybrid plasmonic modes. Compared to the traditional hybrid plasmon polaritons, they offer different advantages to nanolaser applications. The laser's properties could be effectively tuned by controlling the tip angle of the metallic substrate, and laser actions with improved optical performance could be realized. Reduced pumping threshold or miniaturized generated coherent optical fields may be achieved through using different waveguide schemes.

2. Plasmon nanolasers based on triangular metal grooves

The theoretical model of the proposed metal-groove based plasmon nanolaser is shown schematically in Fig. 1, where a CdS nanowire (acting as the gain medium) sits above a silver groove substrate, separated by a nanometer MgF_2 gap of thickness t. (Here the nanowire is assumed to be at the bottom center of the MgF_2 coated silver groove). The radius of the nanowire is r and the tip angle of the triangular silver groove substrate is θ (corresponding to the range of $180^\circ < \theta < 360^\circ$). The tip radius of the bottom corner of the metal groove in the waveguiding structure is considered as rounded of a fixed 10 nm. The lasing wavelength is set at $\lambda = 489$ nm, which corresponds to the CdS I_2 exciton line. The permittivities of CdS, MgF_2, air and Ag are 5.76, 1.96, 1 and $-9.2+0.3i$ [69], respectively. The modal properties of the structure are investigated by the finite-element method (FEM) using COMSOL™ with the scattering boundary condition.

In previous work, the metal groove structures with sharp angles had been intensively studied as efficient optical components operating at the telecom wavelength to attain the goal of light guiding, mode splitting, wavelength filtering as well as other applications [65,66,68]. In contrast to these CPP waveguiding structures, metal-groove based hybrid waveguide could support well-confined plasmonic modes within a wide-range of tip angles, even for the case when the metal groove by itself does not support a guided channel plasmon polariton mode [58]. Fig. 2(a) and (b) has shown the electric field distributions of the two hybrid plasmonic modes supported by the studied hybrid structure based

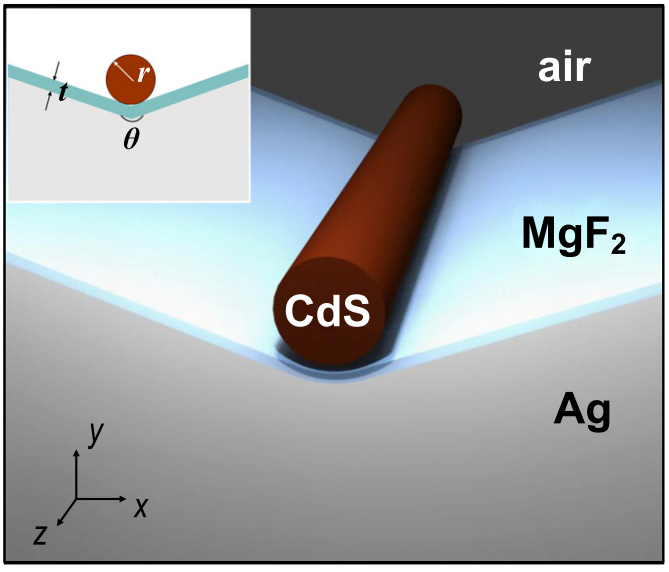

Fig. 1. Geometry of the plasmon nanolaser with a triangular metal groove substrate.

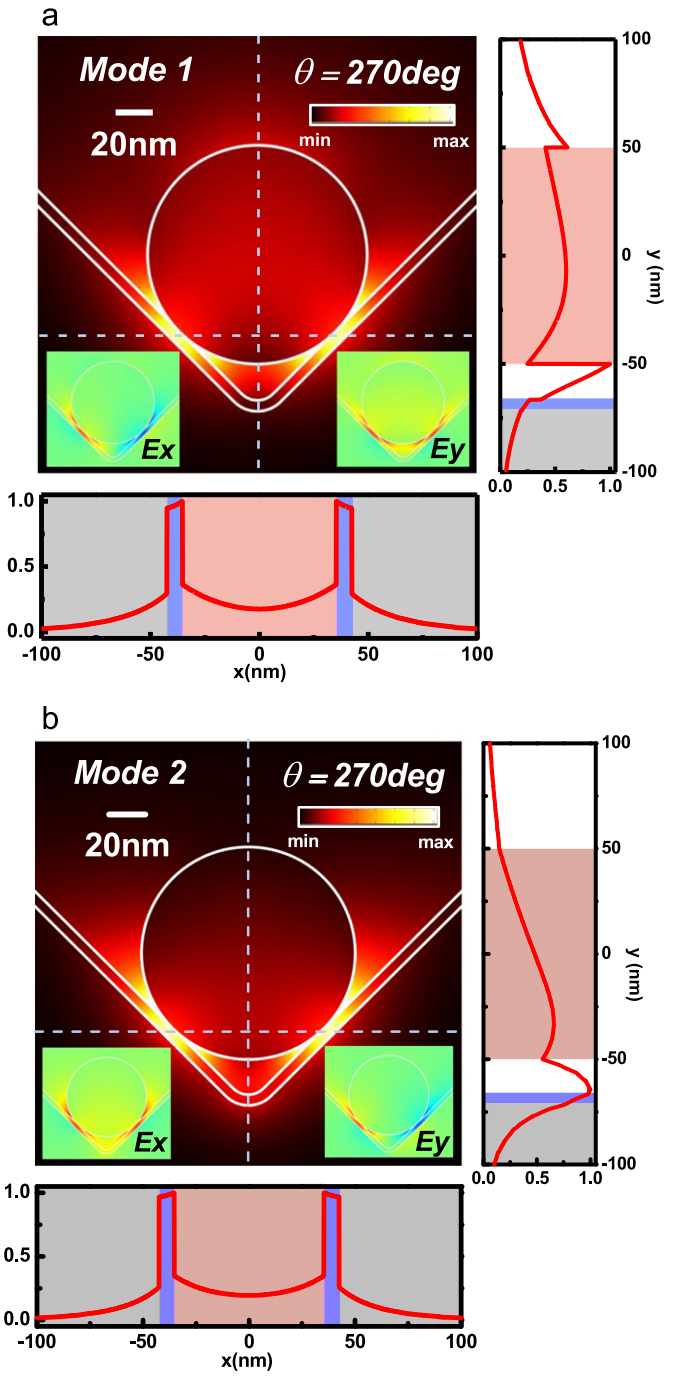

Fig. 2. 2D and cross-sectional (along the dashed-lines in the 2D plot) electric field distributions ($|E(x, y)|$) of the plasmonic modes supported by the metal groove based hybrid structure ($\theta = 270^\circ$, $t = 5$ nm), where the insets illustrate the corresponding Ex and Ey components: (a) Mode 1; (b) Mode 2. The positions of the dashed-lines are determined by the points of tangency between the CdS nanowire and the MgF_2 layer along the x direction, and through the center of the nanowire for the y direction.

on a 270° metallic groove ($t = 5$ nm). Both of the hybrid plasmonic modes exhibit quasi-TEM modal behaviors, with comparable Ex and Ey components (although not equal). The first mode (Mode 1) has a lower effective index, with Ey component larger than the Ex one, thus exhibiting a quasi-TM-like feature. Whereas the second mode (Mode 2) has a higher effective index, and its Ex component is more dominant compared to Ey component, therefore demonstrating a quasi-TE-like modal property. As seen from the cross-sectional electric field plots, for either of the modes, strong

optical confinement can be achieved in the gap regions between the metal sidewalls and the nanowire, and meanwhile with sufficient modal overlap in the CdS region to facilitate gain. While further comparison between the two modes reveals that the field overlap in the gain medium for Mode 1 is more pronounced than Mode 2, indicating stronger mode confinement achieved in the semiconductor nanowire. Along with the feature of lower propagation loss, Mode 1 shows the potential to enable lower pumping threshold for such a specific case (θ=270°), and could thus possibly become the lasing mode when optical gain is provided.

The modal properties of hybrid groove structures with different CdS nanowires (r=40 nm, 50 nm, 60 nm) are then investigated at various tip angles, where the thickness of the MgF_2 is fixed at 5 nm. The real part of the modal effective index (n_{eff}=Re(N_{eff})), effective propagation loss (α_{eff}), normalized mode area (A_{eff}/A_0) and confinement factor (Γ) of the hybrid plasmonic modes of our proposed structure are shown in Fig. 3(a)–(d) as θ varies from 180° to 360°. The effective propagation loss is obtained from the imaginary part of the modal effective index, i.e., α_{eff}=Im(N_{eff}). The confinement factor (Γ) is defined as the ratio of the electric energy in the CdS nanowire and the total electric energy of the mode. The effective mode area is calculated using $A_{eff}=\iint W(\boldsymbol{r})dA/\max(W(\boldsymbol{r}))$ [7,8], which is inversely proportional to the Purcell factor [8]. In order to accurately account for the energy in the metal region, the electromagnetic energy density $W(r)$ is defined as:

$$W(\boldsymbol{r})=\frac{1}{2}\mathrm{Re}\left\{\frac{d[\omega\varepsilon(\boldsymbol{r})]}{d\omega}\right\}|E(\boldsymbol{r})|^2+\frac{1}{2}\mu_0|H(\boldsymbol{r})|^2 \quad (1)$$

In Eq. (1), $E(\boldsymbol{r})$ and $H(\boldsymbol{r})$ are the electric and magnetic fields, $\varepsilon(\boldsymbol{r})$ is the electric permittivity and μ_0 is the vacuum magnetic permeability. A_0 is the diffraction-limited mode area in free space and defined as $\lambda^2/4$.

It is shown clearly in Fig. 3(a) that depending on the value of θ, the hybrid groove structure is able to support the transmission of more than one mode. The extreme case of θ=180° corresponds to the conventional hybrid plasmon laser structure, which allows for a single quasi-TM mode transmission when the CdS nanowire is not too large [5,10] (Such mode is denoted as Mode 1). Increasing θ leads to the decrease of the effective index of Mode 1 and meanwhile results in the emergence of the second mode (named as Mode 2) with increased effective index. When θ evolves from 180° toward 350°, the second mode of the large nanowire case comes out earlier than the smaller one, for example, θ–190° for r=60 nm and θ–230° for r=40 nm. Continuously increasing the tip angle leads to further reduction of the effective index for Mode 1, and finally it reaches cutoff when the nanowire is small (e.g. r=40 nm). It is illustrated in the red solid curves of Fig. 3(a)–(d) that, near the cutoff condition, the effective index is close to 1, while the propagation loss and confinement factor both see a sharp decrease, with the corresponding mode area also undergoing a rapid increase. While for the r=50 nm and r=60 nm cases, the modal properties do not experience any rapid change since Mode 1 is far away from cutoff. On the other hand, for all the studied nanowire radii, the propagation loss of Mode 2 increases first before it decreases, while the mode area decreases first before it increases correspondingly. The confinement factor always experiences an increase with larger θ due to the increasingly enhanced confinement, indicating more overlap between the hybrid mode and the gain medium, which is beneficial for practical applications. We also note from the calculated field profiles that Mode 1 undergoes a change in its dominant polarization during the increase of the tip angle, i.e., from quasi-TM-like behavior at 180° to an asymmetric quasi-TE-like character (e.g. when θ exceeds 295° for r=50 nm). On the other hand, Mode 2 also experiences a polarization conversion, evolving quickly from the Ey-dominant

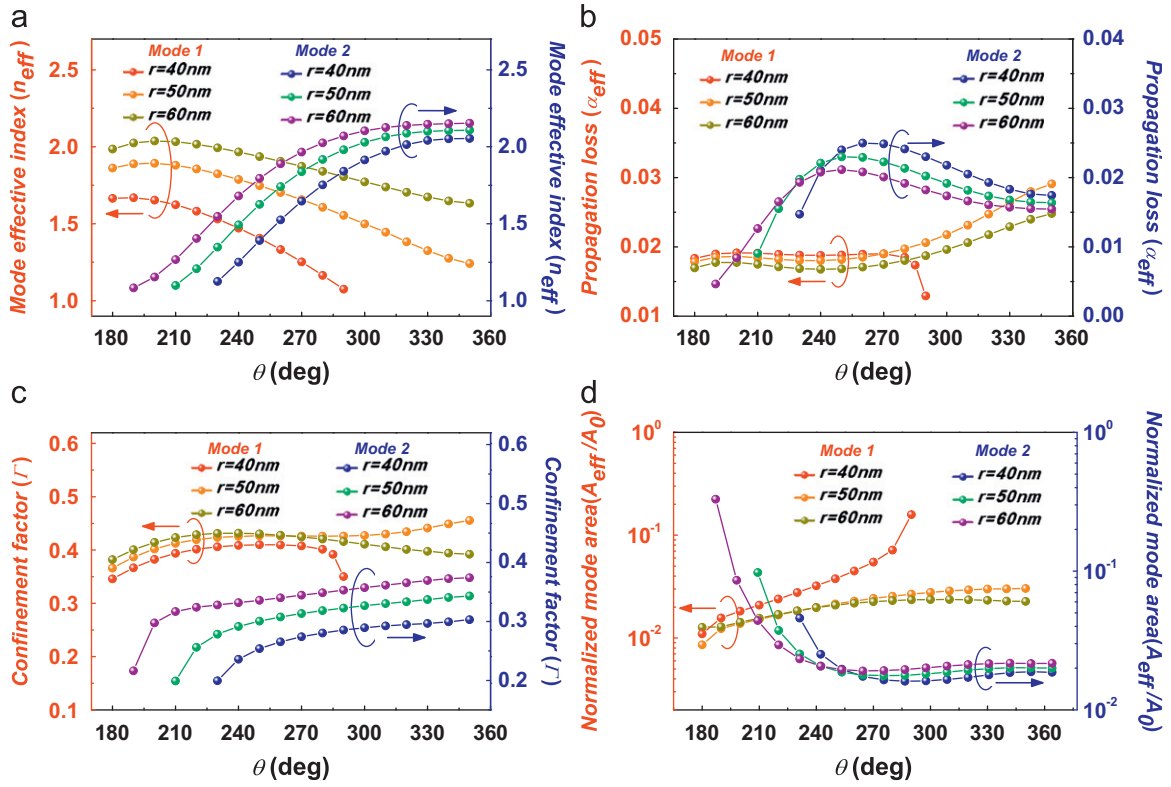

Fig. 3. Modal properties of the hybrid plasmonic modes at different θ: (a) Modal effective index (n_{eff}); (b) effective propagation loss (α_{eff}); (c) normalized mode area (A_{eff}/A_0); (d) confinement factor (Γ). The left and right coordinates correspond to the results of Mode 1 and Mode 2, respectively. (For interpretation of the references to color in this figure, the reader is referred to the web version of this article.)

mode at the beginning into a symmetric quasi-TE-like modal behavior (e.g. $\theta > 240^\circ$ for $r=50$ nm). It is also illustrated from Fig. 3(c) that the mode area of Mode 1 of the hybrid groove structure is larger than the conventional plasmon laser based on a flat metallic substrate (see $\theta=180^\circ$ in the figure), indicating its Purcell factor would be smaller than the conventional one. However, for Mode 2, its mode area can be smaller than the 180° case, indicating a larger Purcell factor is achievable.

Based on the above modal analysis, we then investigated the pumping thresholds needed to enable lasing actions for the two modes. The threshold, determined by two factors, can be calculated using $g_{th}=g_1+g_2=k_0\alpha_{eff}/\Gamma\ (n_{eff}/n_{wire})+\ln(1/R)/L/\Gamma\ (n_{eff}/n_{wire})=(k_0\alpha_{eff}+\ln(1/R)/L)/\Gamma\ (n_{eff}/n_{wire})$ [10], where $k_0=2\pi/\lambda$ and n_{wire} is the refractive index of the nanowire. The length of the nanowire (L) is set to be 30 μm, while the reflectivity is estimated to be $R=(n_{eff}-1)/(n_{eff}+1)$. These definitions are the same as in [10]. The first part of g_{th}, i.e., $g_{1,}$, is related to the metallic loss (propagation loss), while the second part (i.e., g_2) is strongly associated with the cavity loss. It can be seen from Fig. 4(a) and (b) that the value of g_1 is typically larger than g_2, thus playing a more dominant role in determining the ultimate lasing threshold. The calculated results of g_{th} in Fig. 4(c) illustrate which mode will be the lasing mode is highly dependent on the exact tip angle of the metal groove substrate. For $r=40$ nm, the amplitude threshold gain of Mode 1 is substantially lower than that of Mode 2. Thus Mode 1 would be the lasing mode as long as it is not cutoff, and the

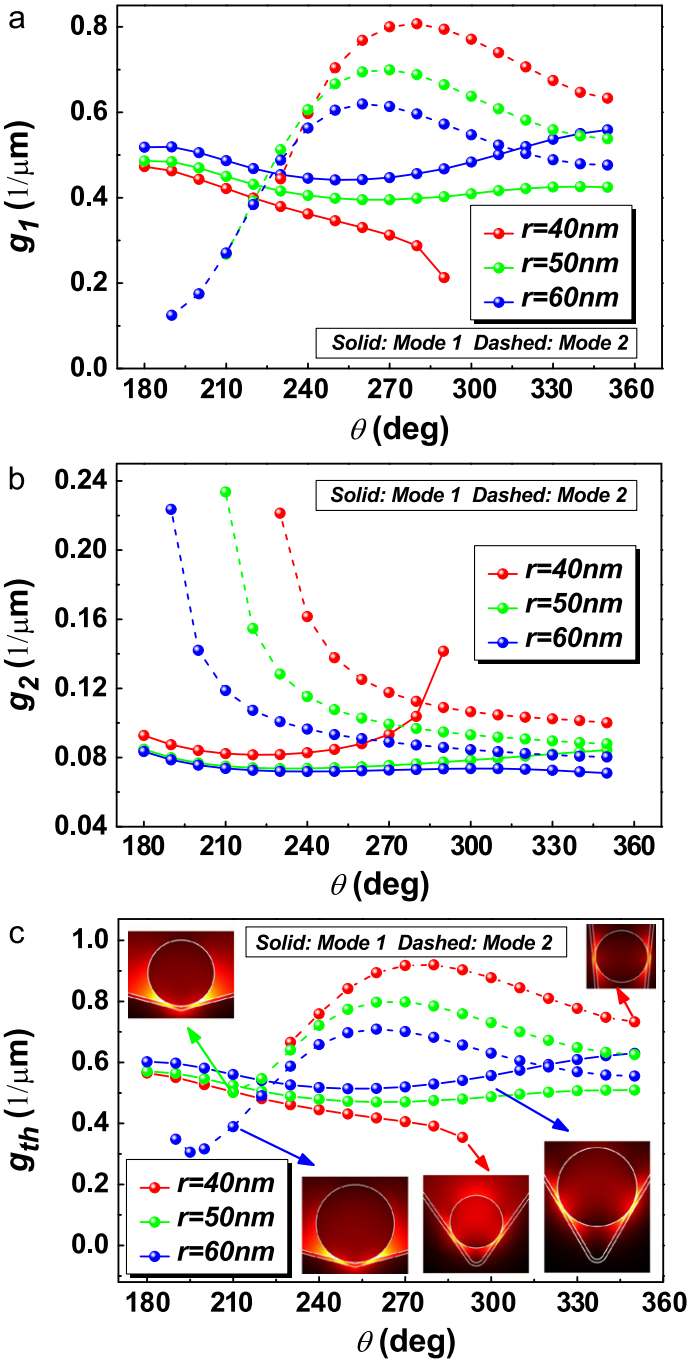

Fig. 4. (a)–(c) g_1, g_2 and lasing thresholds (g_{th}) of the two modes for various θ, where the insets plot the corresponding electric field distributions in (c). Solid curves correspond to Mode 1 while dashed curves represent Mode 2. Upper insets, from left to right: $r=50$ nm, $\theta=210^\circ$; $r=40$ nm, $\theta=350^\circ$; lower insets, from left to right: $r=60$ nm, $\theta=210^\circ$; $r=40$ nm, $\theta=290^\circ$; $r=60$ nm, $\theta=300^\circ$.

corresponding threshold decreases monotonically with larger θ. When θ exceeds a critical value, Mode 2 will become the only guided mode supported by the structure. Therefore it will lase if optical gain is provided. When $r=50$ nm, Mode 1 will be the lasing mode for most of the cases, as it has lower pumping threshold. Only when θ is around 210° does Mode 2 show the possibility to enable laser action. For such a nanowire radius, the threshold undergoes a moderate change within the considered angle range, exhibiting near-stable lasing properties. While for $r=60$ nm, the situations becomes much more complicated (See the blue curves). Mode 2 has a lower pump threshold when θ is either very small or very large, thus will lase when optical gain reaches the threshold. Conversely, when θ has a moderate value, Mode 1 would be the lasing mode as the gain needed for laser action is much lower than that of Mode 2. Compared to the conventional plasmon laser based on flat metallic substrate (corresponding to the case of $\theta=180°$ shown in Fig. 4), reduced lasing threshold is always achievable with appropriately selected tip angle for the studied hybrid metal groove structures, indicating improved lasing properties could be obtained through engineering the angle of the substrate. Another unique property is the polarization diversity of the optical mode yielded by the plasmon laser, which could also be readily controlled by choosing specific tip angles.

Here it is worth mentioning that, when the tip angle is very large (e.g. 350°), the hybrid structure is able to support more than two plasmonic modes. However, due to the fact that these modes are generated from the coupling between the higher order CPP modes and the nanowire mode, the modal overlap with the semiconductor material is very low, thus requiring substantially huge threshold gain to enable laser actions. For simplicity, we did not include the discussions of their modal properties in the above analysis.

3. Plasmon nanolasers based on triangular metal wedges

Another type of plasmon lasers considered here is based on metal wedge structures, which have been studied with the capability of achieving ultra-deep-subwavelength mode confinement and relatively low propagation loss [43]. The geometry is shown in Fig. 5, where the tip angle of the triangular silver wedge substrate is θ (set within the range of $20° < \theta < 180°$) and other parameters are denoted the same as that for the metal groove based structure. The tip radius of the metal wedge is assumed to be rounded with a fixed curvature of 10 nm. Although fabrication of the wedge-type plasmonic structure is more challenging than the groove-based configuration in a certain aspect, it is still interesting to investigate the optical performances of such a structure when leveraged in nanolaser applications, since the wedge substrate could add some unique features, such as further scaling down the yielded mode size and enabling single-mode operations when the CdS nanowire is not very large. In Fig. 6, the electric field of the hybrid wedge plasmonic mode supported by the structure is shown well concentrated within the ultra-thin MgF_2 gap layer near the wedge tip due to the strong hybridization between the wedge plasmonic mode and the dielectric nanowire mode, which indicates an ultra-small mode area achievable and meanwhile exhibiting reasonable modal overlap with the gain medium to enable laser action. Such a deep-subwavelength-scale mode size offers unique advantages to allow electronic transitions directly coupled to strongly confined optical modes, thus overcoming the challenge of delivering light from microscopic external sources into a deep-subwavelength scale.

Calculated modal properties of the wedge-type laser structures are shown in Fig. 7(a) and (b). It is clearly illustrated that similar modal behaviors are achieved for different nanowire sizes when θ grows from 20° to 180°. Here the case of 180° corresponds to the conventional flat metal substrate based plasmon laser. For most of the cases, both the modal effective index and the propagation loss decrease with increased tip angle. The only exception occurs when θ gets close to 180° (e.g. θ: 160°–180°), where α_{eff} increases slightly for all the studied r while the decreasing trend of n_{eff} slows down and even changes reversely into an increasing behavior for the large nanowire case (e.g. $r=50$ nm and 60 nm). The confinement factor, however, exhibits a monotonical trend with the change of the tip angle all the time, which reaches its maximum when θ equals 180°. As also indicated from Fig. 7(b), ultra-deep-subwavelength mode area is achievable when the tip angle is relatively small, which could be leveraged to enable the operation of a plasmon laser with nanoscale optical mode size.

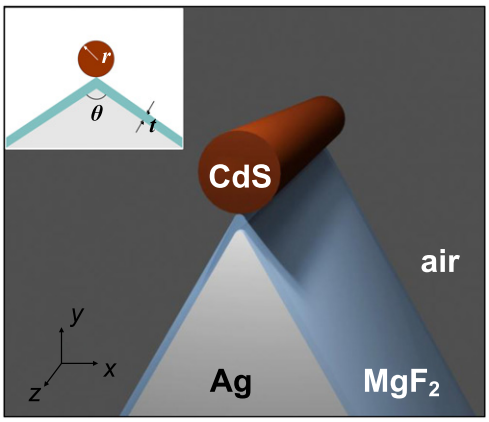

Fig. 5. Geometries of the plasmon nanolaser based on a triangular metal wedge substrate.

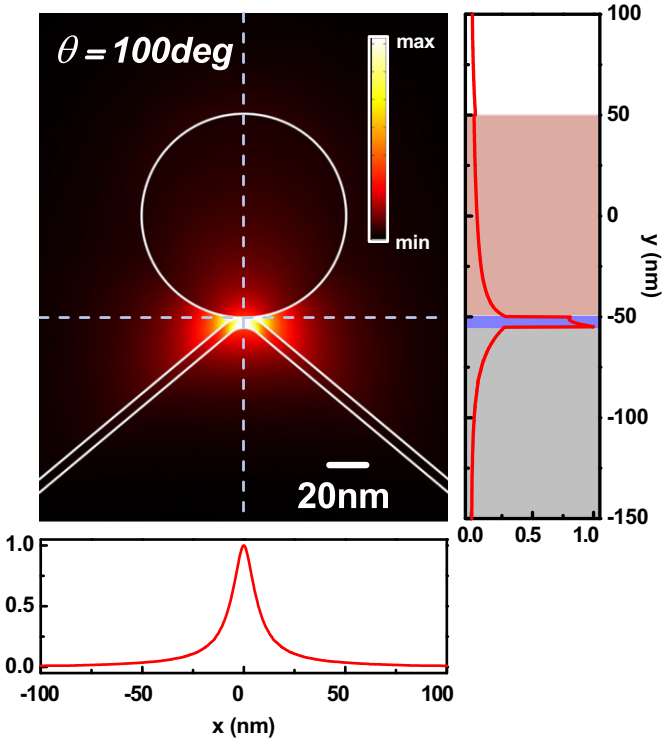

Fig. 6. 2D and cross-sectional (along the dashed-lines in the 2D plot) electric field distributions ($|E(x, y)|$) of the plasmonic modes supported by the metal groove based hybrid structure ($\theta=60°$, $t=5$ nm). The positions of the dashed-lines are determined by the points of tangency between the CdS nanowire and the MgF_2 layer along the x direction, and through the center of the nanowire for the y direction.

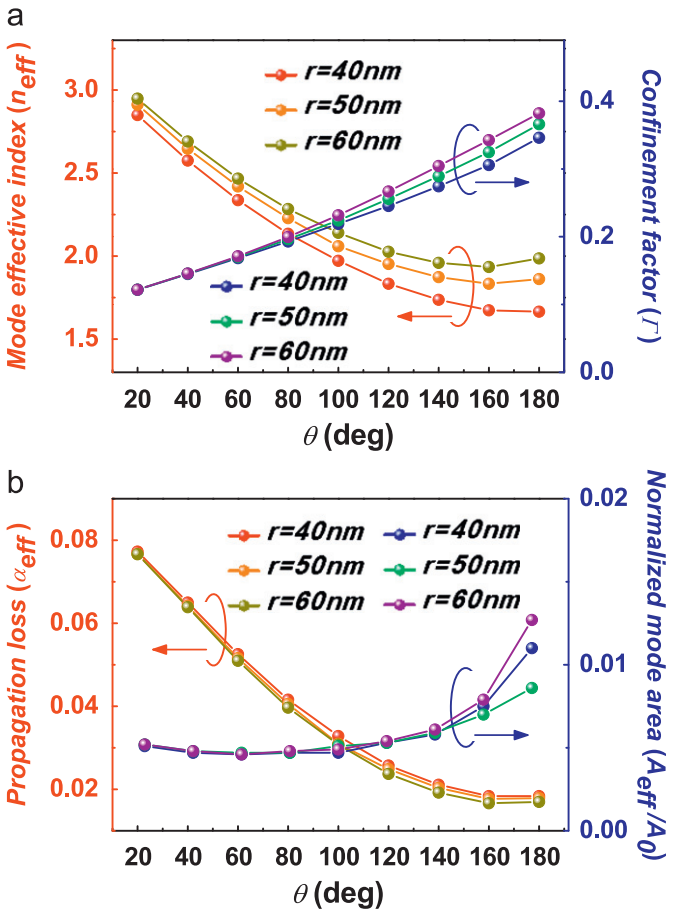

Fig. 7. Modal properties of the hybrid plasmonic mode versus the variation of θ: (a) modal effective index and confinement factor; (b) effective propagation loss and normalized mode area.

The reduced mode size also indicates a larger Purcell factor might be achieved using the metal-wedge-based-plasmon nanolaser when compared to the flat-metal-substrate-based structure.

Fig. 8(a)–(c) demonstrates the results of g_1, g_2 and the needed threshold gain (g_{th}) for laser actions, where the electric field distributions of yielded optical modes for typical configurations are also drawn in the insets in Fig. 8(c). Similar to the metal groove based structure, the effect of g_1 (caused by metallic loss) is more dominant than g_2 (caused by cavity loss). It is shown in Fig. 8(c) that the calculated pumping threshold is seen dependent more strongly on the tip angle of the metal wedge substrate than the nanowire radius. Due to the reduced modal overlap with the gain medium and increased propagation loss, the threshold at small θ is relatively large. However, as long as optical gain reaches the threshold, the only confined hybrid wedge plasmonic mode can still lase, thus enabling the realization of ultra-deep-subwavelength plasmon lasers.

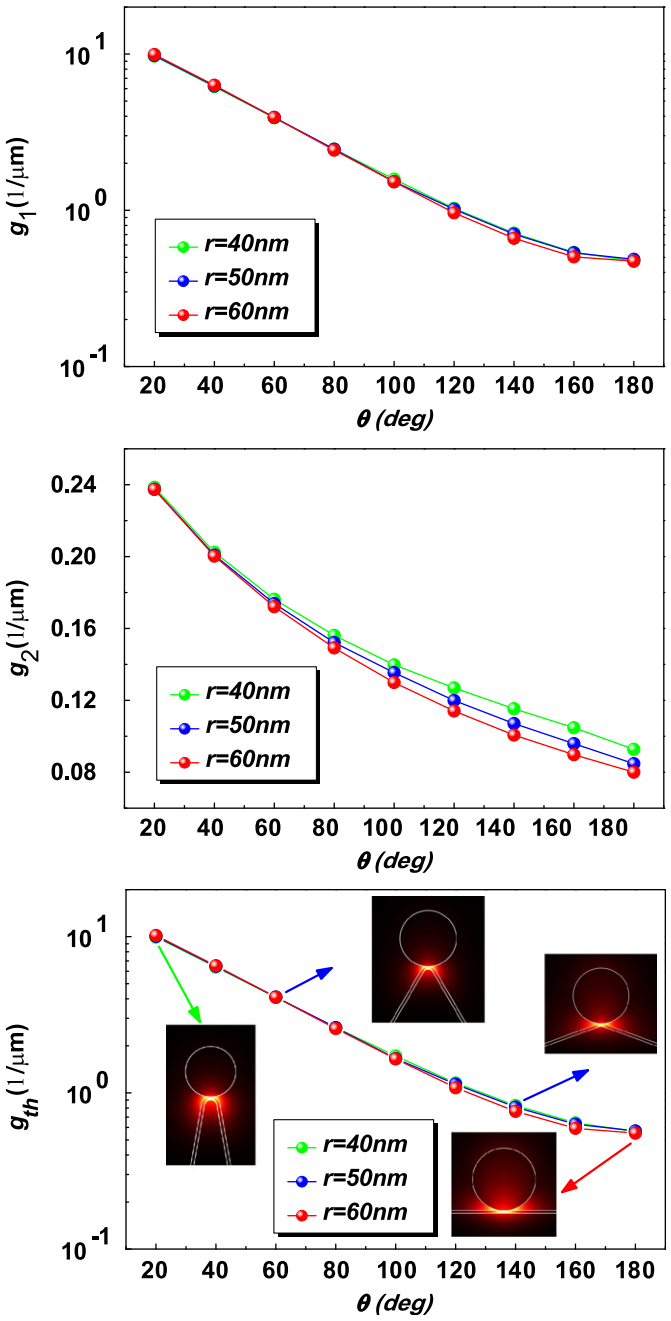

Fig. 8. (a)–(c) Dependence of g_1, g_2 and lasing threshold (g_{th}) on θ, where the insets plot the corresponding electric field distributions in (c). Upper insets, from left to right: r=60 nm, θ=60°; r=60 nm, θ=140°; lower insets, from left to right: r=40 nm, θ=20°; r=50 nm, θ=180°.

4. Conclusions

In this paper, we have investigated novel plasmonic structures for nanolasers' applications. Through numerical simulations, we show that the laser's properties could be effectively tuned by controlling the tip angle of the metallic substrate. Owning to the enhanced optical confinement, hybrid structures with metal groove substrates could operate with lower lasing thresholds than the conventional counterparts based on flat metallic surfaces. While on the other hand, metal wedge based hybrid plasmonic structures could be used to generate and deliver deep-subwavelength-size optical mode, yet meanwhile coming at a price of relatively high lasing thresholds. These hybrid plasmonic structures with flexible optical properties may find useful applications in active integrated photonic systems.

Acknowledgments

The work at Beihang University was supported by 973 Program (2009CB930702), NSFC (61221061/61077064), National key scientific instruments and equipment development special fund management (2011YQ0301240502) and Scholarship Award for Excellent Doctoral Student granted by Ministry of Education at Beihang University.

References

[1] R. Kirchain, L. Kimerling, Nature Photonics 1 (2007) 303.
[2] W.L. Barnes, A. Dereux, T.W. Ebbesen, Nature 424 (2003) 824.
[3] D.K. Gramotnev, S.I. Bozhevolnyi, Nature Photonics 4 (2010) 83.
[4] M.A. Noginov, G. Zhu, A.M. Belgrave, R. Bakker, V.M. Shalaev, E.E. Narimanov, S. Stout, E. Herz, T. Suteewong, U. Wiesner, Nature 460 (2009) 1110.
[5] R.F. Oulton, V.J. Sorger, T. Zentgraf, R.M. Ma, C. Gladden, L. Dai, G. Bartal, X. Zhang, Nature 461 (2009) 629.
[6] R.-M. Ma, R.F. Oulton, V.J. Sorger, G. Bartal, X. Zhang, Nature Materials 10 (2011) 110.
[7] R.F. Oulton, V.J. Sorger, D.A. Genov, D.F.P. Pile, X. Zhang, Nature Photonics 2 (2008) 496.
[8] R.F. Oulton, G. Bartal, D.F.P. Pile, X. Zhang, New Journal of Physics 10 (2008) 105018.
[9] V.J. Sorger, Z. Ye, R.F. Oulton, Y. Wang, G. Bartal, X. Yin, X. Zhang, Nature Communications 2 (2011) 331.
[10] L. Zhu, IEEE Photonics Technology Letters 22 (2010) 535.
[11] M.Z. Alam, J. Meier, J.S. Aitchison, M. Mojahedi, Super Mode Propagation in Low Index Medium, Conference on Laser and Electro-Optics IEEE 2007, pp. Paper JThD112.
[12] M. Fujii, J. Leuthold, W. Freude, IEEE Photonics Technology Letters 21 (2009) 362.
[13] D.X. Dai, S.L. He, Optics Express 17 (2009) 16646.
[14] Y.S. Bian, Z. Zheng, X. Zhao, J.S. Zhu, T. Zhou, Optics Express 17 (2009) 21320.
[15] B.F. Yun, G.H. Hu, Y. Ji, Y.P. Cui, Journal of the Optical Society of America B 26 (2009) 1924.
[16] X. Guo, M. Qiu, J. Bao, B.J. Wiley, Q. Yang, X. Zhang, Y. Ma, H. Yu, L. Tong, Nano Letters 9 (2009) 4515.
[17] I. Avrutsky, R. Soref, W. Buchwald, Optics Express 18 (2010) 348.
[18] X.Y. Zhang, A. Hu, T. Zhang, X.J. Xue, J.Z. Wen, W.W. Duley, Applied Physics Letters 96 (2010) 043109.
[19] M. Wu, Z.H. Han, V. Van, Optics Express 18 (2010) 11728.
[20] H.S. Chu, E.P. Li, P. Bai, R. Hegde, Applied Physics Letters 96 (2010) 221103.
[21] Y.S. Zhao, L. Zhu, Journal of the Optical Society of America B 27 (2010) 1260.
[22] M.Z. Alam, J. Meier, J.S. Aitchison, M. Mojahedi, Optics Express 18 (2010) 12971.
[23] Y. Song, J. Wang, Q.A. Li, M. Yan, M. Qiu, Optics Express 18 (2010) 13173.
[24] D.X. Dai, S.L. He, Optics Express 18 (2010) 17958.
[25] X.Y. Zhang, A. Hu, J.Z. Wen, T. Zhang, X.J. Xue, Y. Zhou, W.W. Duley, Optics Express 18 (2010) 18945.
[26] P.D. Flammer, J.M. Banks, T.E. Furtak, C.G. Durfee, R.E. Hollingsworth, R.T. Collins, Optics Express 18 (2010) 21013.
[27] I. Goykhman, B. Desiatov, U. Levy, Applied Physics Letters 97 (2010) 141106.
[28] Y.S. Bian, Z. Zheng, Y. Liu, J.S. Zhu, T. Zhou, Optics Express 18 (2010) 23756.
[29] J. Tian, Z. Ma, Q.A. Li, Y. Song, Z.H. Liu, Q. Yang, C.L. Zha, J. Akerman, L.M. Tong, M. Qiu, Applied Physics Letters 97 (2010) 231121.
[30] D. Chen, Applied Optics 49 (2010) 6868.
[31] S.Y. Zhu, G.Q. Lo, D.L. Kwong, Optics Express 18 (2010) 27802.
[32] M.S. Kwon, Optics Express 19 (2011) 8379.
[33] S.Y. Zhu, T.Y. Liow, G.Q. Lo, D.L. Kwong, Optics Express 19 (2011) 8888.
[34] Y. Kou, F. Ye, X. Chen, Optics Express 19 (2011) 11746.
[35] J. Zhang, L. Cai, W. Bai, Y. Xu, G. Song, Optics Letters 36 (2011) 2312.
[36] Y.S. Bian, Z. Zheng, Y. Liu, J.S. Zhu, T. Zhou, IEEE Photonics Technology Letters 23 (2011) 884.
[37] H. Benisty, M. Besbes, Journal of Applied Physics 108 (2010) 063108.
[38] X. Sun, L. Zhou, X. Li, Z. Hong, J. Chen, Applied Optics 50 (2011) 3428.
[39] Y.L. Su, Z. Zheng, Y.S. Bian, Y. Liu, J.S. Liu, J.S. Zhu, T. Zhou, Micro and Nano Letters 6 (2011) 643.
[40] C. Horvath, D. Bachman, M. Wu, D. Perron, V. Van, IEEE Photonics Technology Letters 23 (2011) 1267.
[41] J. Xiao, J.S. Liu, Z. Zheng, Y.S. Bian, G.J. Wang, Journal of Optics 13 (2011).
[42] J.T. Kim, IEEE Photonics Technology Letters 23 (2011).
[43] Y.S. Bian, Z. Zheng, Y. Liu, J.S. Zhu, T. Zhou, Optics Express 19 (2011) 22417.
[44] X. He, L. Yang, T. Yang, Optics Express 19 (2011) 12872.
[45] H.S. Chu, Y.A. Akimov, P. Bai, E.P. Li, Journal of the Optical Society of America B 28 (2011) 2895.
[46] L. Chen, X. Li, G.P. Wang, W. Li, S.H. Chen, L. Xiao, D.S. Gao, Journal of Lightwave Technology 30 (2012) 163.
[47] M.Z. Alam, J.S. Aitchison, M. Mojahedi, Optics Letters 37 (2012) 55.
[48] C.-L. Zou, F.-W. Sun, C.-H. Dong, Y.-F. Xiao, X.-F. Ren, L. Lv, X.-D. Chen J.-M. Cui, Z.-F. Han, G.-C. Guo, IEEE Photonics Technology Letters 24 (2012) 434.
[49] C.-C. Huang, Hybrid plasmonic waveguide comprising a semiconductor nanowire and metal ridge for low-loss propagation and nanoscale confinement, IEEE Journal of Selected Topics in Quantum Electronics, submitted for 18 (2012) 1661.
[50] Y.S. Bian, Z. Zheng, X. Zhao, Y.L. Su, L. Liu, J.S. Liu, J.S. Zhu, T. Zhou, IEEE Photonics Technology Letters 24 (2012) 1279.
[51] V.D. Ta, R. Chen, H.D. Sun, Optics Express 19 (2011) 6.
[52] X. Zuo, Z. Sun, Optics Letters 36 (2011) 2946.
[53] Y.S. Bian, Z. Zheng, X. Zhao, L. Liu, J.S. Liu, J.S. Zhu, T. Zhou, Nanowire based hybrid plasmonic structures for low-threshold lasing at the subwavelength scale, Optics Communications 287 (2013) 245.
[54] B. Min, E. Ostby, V. Sorger, E. Ulin-Avila, L. Yang, X. Zhang, K. Vahala, Nature 457 (2009) 455.
[55] S.V. Boriskina, B.M. Reinhard, Proceedings of the National Academy of Sciences of the United States of America 108 (2011) 3147.
[56] M. Chamanzar, A. Adibi, Optics Express 19 (2011) 22292.
[57] W. Ahn, S.V. Boriskina, Y. Hong, B.M. Reinhard, ACS Nano 6 (2012) 951.
[58] Y.S. Bian, Z. Zheng, X. Zhao, Y.L. Su, L. Liu, J.S. Liu, J.S. Zhu, T. Zhou, Highly confined hybrid plasmonic modes guided by nanowire-embedded-metal grooves for low-loss propagation at 1550 nm, IEEE Journal of Selected Topics in Quantum Electronics, http://dx.doi.org/10.1109/JSTQE.2012.2212002, in press.
[59] D.F.P. Pile, T. Ogawa, D.K. Gramotnev, T. Okamoto, M. Haraguchi, M. Fukui, S. Matsuo, Applied Physics Letters 87 (2005) 061106.
[60] E. Moreno, S.G. Rodrigo, S.I. Bozhevolnyi, L. Martin-Moreno, F.J. Garcia-Vidal, Physical Review Letters 100 (2008) 023901.
[61] A. Boltasseva, V.S. Volkov, R.B. Nielsen, E. Moreno, S.G. Rodrigo, S.I. Bozhevolnyi, Optics Express 16 (2008) 5252.
[62] M. Yan, M. Qiu, Journal of the Optical Society of America B 24 (2007) 2333.
[63] Z. Pan, J. Guo, R. Soref, W. Buchwald, G. Sun, Journal of the Optical Society of America B 29 (2012) 340.
[64] J. Dintinger, O.J.F. Martin, Optics Express 17 (2009) 2364.
[65] S.I. Bozhevolnyi, V.S. Volkov, E. Devaux, T.W. Ebbesen, Physical Review Letters 95 (2005) 046802.
[66] S.I. Bozhevolnyi, V.S. Volkov, E. Devaux, J.Y. Laluet, T.W. Ebbesen, Nature 440 (2006) 508.
[67] V.A. Zenin, V.S. Volkov, Z. Han, S.I. Bozhevolnyi, E. Devaux, T.W. Ebbesen, Journal of the Optical Society of America B 28 (2011) 1596.
[68] V.S. Volkov, S.I. Bozhevolnyi, E. Devaux, J.Y. Laluet, T.W. Ebbesen, Nano Letters 7 (2007) 880.
[69] P.B. Johnson, R.W. Christy, Physical Review B 6 (1972) 4370.